University of Nebraska - Lincoln
DigitalCommons@University of Nebraska - Lincoln

Axel Enders Publications | Research Papers in Physics and Astronomy

1-1-2005

Spin-dependent transport in Fe and Fe/Au multilayers

T. L. Monchesky
Simon Fraser University

Axel Enders
University of Nebraska-Lincoln, a.enders@me.com

R. Urban
Simon Fraser University

K. Myrtle
Simon Fraser University

B. Heinrich
Simon Fraser University

See next page for additional authors

Follow this and additional works at: http://digitalcommons.unl.edu/physicsenders

Part of the Physics Commons

Monchesky, T. L.; Enders, Axel; Urban, R.; Myrtle, K.; Heinrich, B.; Zhang, X.-G.; Butler, W. H.; and Kirschner, J., "Spin-dependent transport in Fe and Fe/Au multilayers" (2005). *Axel Enders Publications.* Paper 6.
http://digitalcommons.unl.edu/physicsenders/6

This Article is brought to you for free and open access by the Research Papers in Physics and Astronomy at DigitalCommons@University of Nebraska - Lincoln. It has been accepted for inclusion in Axel Enders Publications by an authorized administrator of DigitalCommons@University of Nebraska - Lincoln.

Authors
T. L. Monchesky, Axel Enders, R. Urban, K. Myrtle, B. Heinrich, X.-G. Zhang, W. H. Butler, and J. Kirschner

This article is available at DigitalCommons@University of Nebraska - Lincoln: http://digitalcommons.unl.edu/physicsenders/6

Spin-dependent transport in Fe and Fe/Au multilayers

T. L. Monchesky, A. Enders, R. Urban, K. Myrtle, and B. Heinrich
Department of Physics, Simon Fraser University, Burnaby, British Columbia, Canada, V5A 1S6

X.-G. Zhang
Metals and Ceramics Division, Oak Ridge National Laboratory, P.O. Box 2008, Oak Ridge, Tennessee 37831-6114, USA

W. H. Butler*
Center for Materials for Information Technology and Department of Physics and Astronomy, University of Alabama, Box 870209, Tuscaloosa, Alabama 35487-0209, USA

J. Kirschner
Max-Planck-Institut für Mikrostrukturphysik, Weinberg 2, D-06120 Halle, Germany
(Received 30 March 2005; published 30 June 2005)

In situ resistance measurements of epitaxial Fe layers and Au/Fe bilayers were used to quantify the scattering in giant magnetoresistance (GMR) spin valve structures. The semiclassical Boltzmann transport equation, incorporating first-principles local density functional calculations, fitted the thickness dependence of the conductivity. Fits to the data indicate that Fe has a large spin asymmetry with bulk relaxation times $\tau_{\downarrow}=3.0\times10^{-14}$ s and $\tau_{\uparrow}=2.5\times10^{-15}$ s. These give a conductivity equal to that of bulk Fe. The interface scattering from the Fe/GaAs, the Fe/vacuum, and the Au/vacuum interfaces is purely diffuse. This is in contrast to the high electron reflection coefficients determined from kinematical calculations using scanning tunneling microscope images. Fits to conductivity measurements of Au/Fe/GaAs(001) indicate that the Au films have the conductivity of bulk material modified only by interface scattering. The GMR of Au/Fe/Au/Fe/GaAs(001) structures is 1.8% at room temperature and 2.9% at 10 K. The magnetoresistance is reduced by the presence of partial diffuse scattering at the inner interfaces, as indicated by the fits to both the GMR and the Au conductivity. The GMR in Fe/Au structures is intrinsically low due to a large electron band mismatch between Au and Fe band structures.

DOI: 10.1103/PhysRevB.71.214440 PACS number(s): 75.47.De, 75.70.Cn, 72.25.Mk, 72.15.Lh

I. INTRODUCTION

Although it is known that giant magnetoresistance (GMR) is a result of spin-dependent scattering inside magnetic multilayers, a detailed understanding of the physics is still lacking. The role of interface scattering is still under debate. The importance of interface scattering was demonstrated by a series of experiments where foreign atoms were placed at the interfaces between magnetic and nonmagnetic layers.[1,2] The role of interface roughness, however, appears to be system dependent. Suzuki *et al.*[3] found that an increase in the interface roughness, created by annealing, increased the residual resistivity of the Co/Cu/Co layers, but did not significantly affect the GMR, from which they concluded that the magnetoresistance was predominantly due to bulk scattering. Other researchers found that by increasing the interface roughness in Co/Cu multilayers, the magnetoresistance was lowered.[4] In Fe/Cr multilayers, the GMR increased with increasing interface roughness.[5,6] By fitting experimental Fe/Cr data to model calculations, Levy *et al.*[7] estimated that the ratio of bulk to interface scattering in these systems is 0.83.

Given the wide range of behaviors found in experiment, we chose the simplest possible system to investigate quantitatively the spin-dependent scattering in GMR structures. We chose Fe on GaAs as a template since Fe grows in a near layer-by-layer fashion on GaAs(001). GaAs substrates are readily available in semi-insulating format with large atomic terraces. Au was chosen for the nonmagnetic spacer layer due to its simple electronic structure and its lattice match to Fe. The origin of spin-dependent scattering is elucidated in this paper by modeling the resistance and magnetoresistance of high-quality crystalline Fe, Au/Fe, and Au/Fe/Au/Fe structures grown on GaAs(001). These structures were modeled with the semiclassical Boltzmann transport equation in the relaxation time approximation. Full band structure calculations determined the Bloch velocities and the intrinsic transmission and reflection coefficients. We extracted the phenomenological diffuse scattering parameters from each of the interfaces by fitting the data with the band structure calculations.

The paper is organized as follows. In Sec. II, details of the growth of the crystalline films are presented. In Sec. III the field dependence of the orientation of the magnetic moments was measured by magneto-optic Kerr effect (MOKE) to be able to understand the magnetoresistance in detail. The MOKE and GMR measurements presented are compared to model calculations to enable a quantitative measurement of the exchange coupling that gives rise to the antiparallel orientation of the magnetic moments. One of the major difficulties in a quantitative interpretation of magnetoresistance data from magnetic multilayers is the large number of free parameters that are required. In order to reduce the number of parameters, the conductivity of single layers and bilayers was characterized. The results are presented in Sec. IV.

 ©2005 The American Physical Society

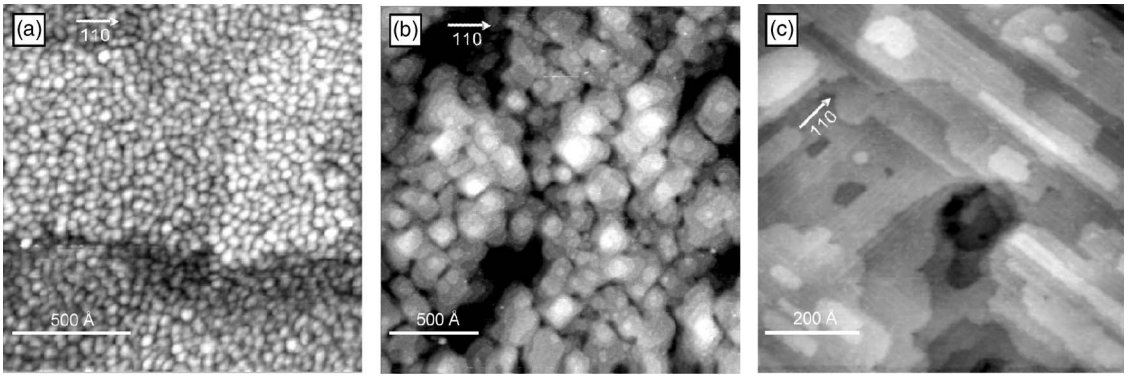

FIG. 1. (a) 150×150 nm^2 STM image of 20 ML Fe/GaAs(001). (b) 200×200 nm^2 STM image of 10 ML Fe grown at 170 °C on Fe/GaAs(001). (c) 78×78 nm^2 STM image of 20 ML Au/28 ML Fe/GaAs(001). The periodic vertical and horizontal lines correspond to the 5×1 reconstruction.

Analysis of the thickness dependence of the conductivity of single Fe layers measured *in situ* gave the bulk scattering rates and the degree of specular scattering at the outer interfaces. The conductivity of Au/Fe bilayers and the GMR of Au/Fe/Au/Fe multilayers enabled a quantitative measure of the spin-dependent scattering at the Fe/Au interfaces and the scattering at the outer interfaces. Section V gives a comparison between the conduction electron scattering at the metal/vacuum interfaces and the scanning tunneling microscope (STM) data.

II. SAMPLE PREPARATION

The samples used for the transport studies were grown on semi-insulating GaAs(001).[8] Scanning tunneling microscopy studies were made using n^+ GaAs substrates.[9] The choice of semi-insulating or heavily doped GaAs did not affect the growth or the magnetic properties. The GaAs surface was prepared by inserting an epiready wafer in ultrahigh vacuum without prior treatment and annealing to roughly 500 °C to desorb the carbon from the substrate. The oxide was removed by 500 eV Ar^+ sputtering at an angle of 75° with respect to the surface normal. Substrates used for the transport studies were rotated about their normal during sputtering. The substrates that were used for the STM studies were not rotated during sputtering, which resulted in a decrease in the quality of the growth as determined by reflection high-energy electron diffraction (RHEED).[9] The sputtering was performed at room temperature (RT) under Auger observation until the contaminants were removed. The sample temperature was gradually raised under RHEED observation until a well-ordered (4×6) reconstruction was obtained at a temperature of roughly 600 °C. Once a well-ordered (4×6) reconstruction was obtained the temperature was lowered to RT, which resulted in no observable change in the reconstruction. See Refs. 8 and 9 for details. STM studies showed that substrates prepared in this fashion have a pseudo (4×6) reconstruction comprised of (1×6) domains and (4×2) domains.[9]

Fe was deposited on RT GaAs from a resistively heated piece of Fe in a base pressure of 1×10^{-10} Torr. The rate of deposition was roughly 1 Å/min as determined by a quartz microbalance. The 10 keV RHEED beam was set to the first anti-Bragg condition for Fe, at a polar angle of 1.1° from the surface. The azimuth was set to 0.8° away from the $[1\bar{1}0]$ direction in order that Kikuchi lines not overlap with the specular spot. The intensity of the specular spot oscillated during the growth with a one monolayer period, allowing accurate determination of the Fe thickness. Sharp RHEED and low-energy electron diffraction spots showed that the Fe was single crystalline with an epitaxial relationship Fe[110]‖GaAs[110]. After the deposition of a 20 monolayer (ML) film, STM images showed an isotropic island distribution, [see Fig. 1(a)]. The separation between island centers was 52 Å, determined from the first minimum in the height difference correlation function. An rms roughness of 1.9 Å was measured across a GaAs terrace.

Arsenic segregates to the Fe surface for all Fe growth on GaAs(001), regardless of the substrate reconstruction or preparation. A comparison of the integrated As $2p_{3/2}$ and Fe As $2p_{3/2}$ x-ray photoelectron spectra (XPS) peaks indicated that there was 0.75 ML of As,[9] where a 1 ML coverage of As is defined here to be the surface density of a GaAs(001) surface, 6.25×10^{14} atoms/cm^2. The weak $c(2\times2)$ reconstruction observed by RHEED provided further evidence of the segregation.

In order to remove the As surfactant from the 20 ML Fe/GaAs(001), the films were sputtered with 500 eV Ar^+ at an angle of 75° with respect to the surface normal. The As $2p_{3/2}$ x-ray photoelectron spectroscopic line was used to monitor the amount of As at the surface; the sputtering was stopped once this peak disappeared. The XPS signal from the clean Fe surface showed that there was no As in the bulk of the Fe layer within the detection limit of XPS, which is roughly 0.1%. In the process of cleaning the surface, 2.2 ML of Fe was removed, as determined from the decrease in the Fe $2p_{3/2}$ peak. In a previous paper we estimated that 0.2 ML of Ga diffused into the Fe as a result of cascade intermixing from the sputtering.[8] However, a more thorough investigation indicated that this was an overestimate. The Ga concentration in the Fe film as a function of Fe film thickness, measured by the ratio of the Ga $2p_{3/2}$ to the Fe $2p_{3/2}$ XPS intensities as a function of the Ar^+ dose, indicated that no more than roughly 0.1% of Ga diffused into the Fe layer.

This result is supported by a Monte Carlo simulation of the sputtering, which showed that the average stopping range for the Ar^+ ions was 4 Å with an ion straggling (second moment of the distribution) of 6 Å.[36]

In order to repair the damage created by sputtering, additional Fe layers were further deposited at a temperature of 200 °C. The RHEED intensity increased by a factor of 3 during the growth of an additional 10 ML Fe and large RHEED intensity oscillations were recovered. The growth at increased temperatures created narrow RHEED streaks indicating an increase in terrace size. STM images of the surface resulting from Fe grown at 170 °C on As-free GaAs is shown in Fig. 1(b). From the height difference correlation function, the average separation between islands was 265 Å. From a calculation of the partial pair correlation functions, the islands could be seen to be composed of a number of terraces 35 Å wide on average. These As-free Fe layers were found to serve as good templates for growing GMR structures. From ferromagnetic resonance (FMR) measurements, the Fe/GaAs(001) layers had the magnetic properties of bulk Fe modified only by interface anisotropies.[8]

Au was thermally evaporated from a crucible, at a rate of roughly 1 ML/min, onto the As-free Fe layers. During the growth the substrate was kept at RT. Weaker RHEED intensity oscillations than typically seen for the growth of Fe on GaAs were found for Au on Fe for thicknesses up to 7 ML. These oscillations, however, gave a calibration of the quartz microbalance that was used to measure the film thickness of films thicker than 20 ML. RHEED patterns indicated that the Au film was single crystalline with an epitaxially relationship Au[100]‖Fe[110]. After a 7 ML deposition, RHEED demonstrated that the Au surface had a weak reconstruction. The RHEED streaks resulting from the reconstruction were not well defined, and were likely created by a transitional state between a 1×1 fcc surface and a 1×5 surface. By the end of a 20 ML deposition a clear 1×5 surface reconstruction was observed.

The STM image shown in Fig. 1(c) was measured on a 20 ML Au film on Fe/GaAs. The 1×5 reconstruction consisted of 0.5 Å high corrugations separated by 14 Å along either the [110] or the $[1\bar{1}0]$ directions (the crystallographic directions are referenced to the Au lattice). A detailed STM study of the reconstruction, given by Binnig,[10] showed that the reconstruction arises from the formation of a hexagonal top layer. The lattice mismatch between the fcc (001) surface and the hexagonal layer leads to a buckling of the surface, which gives rise to the periodic corrugations. The STM image in Fig. 1(c) showed that the direction of the elongation of the Au terraces was correlated to the reconstruction and was elongated along the corrugations. The terraces were roughly 500 Å long and 120 Å wide.

Unlike the Fe deposited on Cu/Fe/GaAs(001),[8] Fe films deposited at RT on Au/Fe/GaAs created strong RHEED intensity oscillations indicative of a smoother growth. For RT growth of Fe/Au(001), an Auger study estimated roughly 1 ML of Au segregated to the surface of Fe.[11] The segregation of Au was further supported by low-energy electron diffraction[12] and photoemission studies.[13] For the case of Fe deposited on Au/Fe/GaAs(001), however, XPS measurements as a function of the top Fe film thickness indicated that Au does not segregate to the surface of Fe.

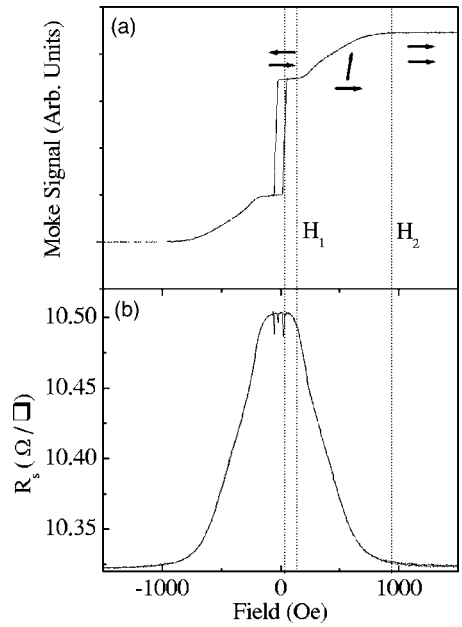

FIG. 2. (a) The Kerr effect and (b) magnetoresistance for the current parallel to the applied field for 20 ML Au/10 ML Fe/7 ML Au/28 ML Fe/GaAs(001), measured at RT. The arrows indicate the orientation of the magnetizations at various stages of the magnetization reversal.

For *ex situ* measurements and characterization, the samples were covered with a 20 ML Au cap to protect them from oxidation. Weak RHEED oscillations were visible for the entire growth allowing for an accurate thickness determination. STM measurements show that the surface of a 20 ML Au film grown on Fe/Au/Fe/GaAs has the same terrace size and reconstruction as the 20 ML Au film grown on As-free Fe on GaAs shown in Fig. 1(c).

III. MAGNETIC CHARACTERIZATION

The magnetoresistance of Fe/Au/Fe was investigated by selecting a thickness suitable to give antiferromagnetic coupling between the Fe layers. For GMR studies, a sample consisting of 20 ML Au/10 ML Fe/7 ML Au/28 ML Fe/GaAs(001) was grown. The sample was photolithographically patterned in order to monitor the magnetoresistance and the longitudinal MOKE over the same portion of the sample. The pattern enabled a four-probe resistance measurement over a 0.5×1.0 mm^2 region. The patterning was achieved by spinning and developing a 2-μm-thick photoresist over the film. A 3 keV Ar^+ beam sputtered away the undesired portions of the film.

In Fig. 2 the field dependence of the sheet resistance and the Kerr signal is plotted, which show a near one-to-one correspondence. The small difference in the field value H_1 for MOKE and magnetoresistance could be explained by inhomogeneities in the spacer thickness. The MOKE measurements were made on a 100-μm-diameter region, whereas GMR measured the coupling over a 0.5×1.0 mm^2 region.

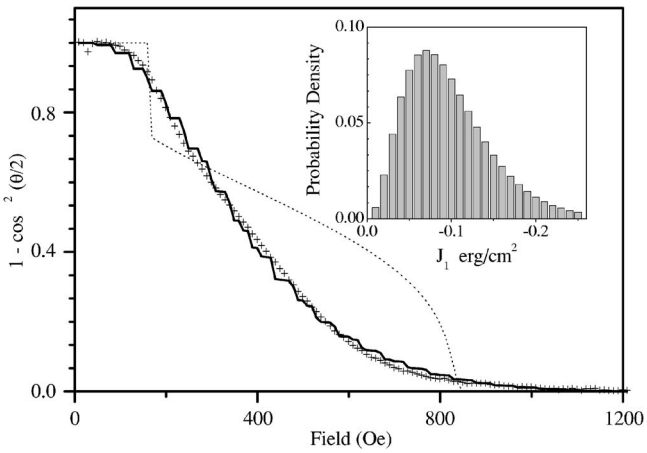

FIG. 3. A fit to the field dependence of the magnetoresistance. The normalized experimental data are show by the points (+). The dashed line is the calculated magnetoresistance for the exchange coupling strengths $J_1=-0.11$ erg/cm^2 and $J_2=0.05$ erg/cm^2. The solid line is a fit to the data with a gamma distribution of bilinear coupling for $J_2=0$. The field dependence of the magnetization configuration for each coupling strength was calculated by minimum-energy calculations.

Two small 0.16% drops in the magnetoresistance were observed near zero applied field. These corresponded to the magnetization rotating from one easy axis to the other during the reversal. These drops, also observed in Fe/Cu/Fe/GaAs, were attributed to anisotropic magnetoresistance.[8]

MOKE measurements showed that the Fe layers were antiferromagnetically coupled, in agreement with measurements made on Fe/Au trilayers grown on Fe(001) whisker substrates.[14] The saturation of the magnetoresistance and the Kerr signal indicated that the two Fe films were parallel for applied fields greater than 1 kOe. The ratio of zero-field Kerr signal to the signal at saturation, 0.53, was roughly equal to the ratio of the difference to the sum of the Fe thicknesses, 0.47. This shows that the films are antiparallel in zero applied field. A more accurate calculation of the MOKE signal accounting for attenuation of the light and reflection from the interfaces predicts a ratio of 0.50.

The strength of the interlayer exchange coupling was measured by fitting the field dependence of the magnetoresistance using minimum energy calculations as described in Ref. 15. The fourfold anisotropies used as input parameters in the fit, $K_1=3.1\times10^5$ and 2.6×10^5 erg/cm^3 were obtained from the anisotropies measured from our previous studies of Fe/GaAs(001),[8] and of Au/Fe/Ag(001) samples.[16] The contribution of the interlayer exchange coupling to the free energy was modeled by bilinear and biquadratic exchange terms of the form $E=-J_1\cos(\theta)+J_2\cos^2(\theta)$, where θ is the angle between the magnetic moments of the two ferromagnetic layers. A single pair of bilinear and biquadratic exchange coupling strengths, $J_1=-0.11$ erg/cm^2 and $J_2=0.05$ erg/cm^2, were able to reproduce the saturation field H_2 and the low-field kink in the GMR curve at a field H_1 as shown by the dashed line in Fig. 3. The simple model, however, did not reproduce the detailed behavior of the field dependence. The rounding of the features at fields H_1 and H_2, indicated in Fig. 2, was due to the inhomogeneity of the coupling strength caused by small variations in the spacer thickness and morphology.

The inhomogeneity of the coupling was modeled by assuming a value for J_2 and calculating the field dependence of the GMR for each value of J_1 in the range 0–0.25 erg/cm^2. A Gaussian distribution of J_1 could not reproduce the data on account that the rounding at H_2 had a smaller curvature than the rounding at H_1: a symmetric distribution rounded the two jumps equally. A gamma distribution of the bilinear coupling was found to give a better fit to the data. A least-squares fit was made to the GMR data, using a gamma probability distribution of the form $P(J_1)=\alpha^M J_1^{M-1}\exp(-\alpha J_1)/\Gamma(M)$ and assuming $J_2=0$. The distribution shown in the inset of Fig. 3 has fitting parameters $\alpha=36$ and $M=3.5$ that correspond to a mean coupling strength of -0.097 erg/cm^2 and a width of roughly 0.04 erg/cm^2. As the biquadratic coupling was increased, the quality of the fit gradually decreased. For values of $J_2>0.03$ erg/cm^2, a low-susceptibility plateau developed in the calculated curve between the fields H_1 and H_2 which did not fit the data.

A comparison between coupling strengths measured on other substrates demonstrated the high quality of the substrates presented here. The coupling strength was considerably larger than the value $J_1=-0.016$ erg/cm^2 obtained on Fe/Au/Fe samples prepared on Ag buffer layers grown directly on GaAs.[17] It was interesting to find that the coupling is only a factor of 2 lower than the coupling strength measured for the highest quality Fe/7 ML Au/Fe samples grown on Fe whisker(001) substrates.[14] The large coupling strength reported in this paper is an indication that the Au/Fe/Au/Fe layers grown directly on GaAs were of high crystalline quality.

The sheet resistance at saturation and zero field was measured between RT and 10 K. From the data in Fig. 2, the sheet resistance at zero applied field $R_s(0)=10.503\ \Omega$ and at saturation $R_s(H_{sat})=10.322\ \Omega$ gave the RT GMR ratio $[R_s(0)-R_s(H_{sat})]/R_s(H_{sat})=1.7\%$. At 10 K the sheet resistances are $R_s(0)=5.312\ \Omega$ and $R_s(H_{sat})=5.161\ \Omega$, which gave a GMR ratio of 2.9%. These are respectable values when comparing to the resistance ratios obtained in $(10\ \text{Å Fe/Au})_{19}$ multilayer structures grown by molecular beam epitaxy. Epitaxial multilayers grown on 470-Å-thick Au buffer layers on GaAs(001) only displayed a RT magnetoresistance of 2.5% for a spacer thickness of 66 Å.[18] Polycrystalline $(9\ \text{Å Fe/Au})_{100}$ multilayers grown on glass substrates showed a magnetoresistance of less than 1% for temperatures between RT and 4 K.[19]

IV. TRANSPORT MEASUREMENTS

A. The model

The thickness dependence of the resistance and the GMR can be used to extract the scattering rates for each spin channel in each layer. However, the free-electron model does not yield a reliable spin asymmetry in scattering because it poorly represents the *d*-band electrons in Fe, which are important in spin-dependent scattering. Furthermore, interface

diffuse scattering can only be extracted if the effects of band mismatch are correctly accounted for. Thus a model using real band structures was needed for the interpretation of our data. For this purpose we used a semiclassical Boltzmann model[20] that incorporates real band structures calculated from first principles. We used the layer Korringa-Kohn-Rostoker (KKR) technique[21] for the *ab initio* electronic structure calculations, which utilizes the two-dimensional periodicity of the layers but does not require any periodicity in the direction perpendicular to the layers. The Bloch wave velocities in the bulk of each layer and the transmission and reflection matrices for each interface were calculated at 16 141 k points in the first Brillouin zone of the two-dimensional reciprocal-lattice space. The results of these calculations were then used as coefficients for the Boltzmann equation.

The solution to the Boltzmann equation yields a deviation function $h(z,\mathbf{k})$ for a metallic multilayer film with the current in the plane of the film. Here the z axis is perpendicular to the film and $\mathbf{k}$ is a wave vector on the Fermi surface. The deviation function is given by the relation $h(z,\mathbf{k})\delta(E_{\mathbf{k}}-E_F) = f(z,\mathbf{k})-f_0(z,\mathbf{k})$, where f is the nonequilibrium electron distribution function, f_0 the equilibrium distribution function, and E_F the Fermi energy. In the relaxation-time approximation, the Boltzmann equation can be solved independently for each value of the momentum parallel to the interfaces, $\mathbf{k}_\parallel=(k_x,k_y)$. The solution in each layer i is given by

$$h_{is}^{\pm,j}(z,\mathbf{k}_\parallel) = -e\tau_{is}\mathbf{v}_{ijs}^{\pm}\cdot\mathbf{E}(1+F_{ijs}^{\pm}e^{\mp z/(\tau_{is}|v_{zijs}^{\pm}|)}), \qquad (1)$$

where $\mathbf{E}$ is the electric field, s indicates the spin channel, and j labels the possible values of momentum perpendicular to the interface, k_z, for a given value of $\mathbf{k}_\parallel$. v_z represents the perpendicular component of the Bloch wave velocity. The solution is divided into currents with positive and negative v_z, denoted $\pm$. The spin-dependent relaxation times in each layer are represented by τ_{is}. The first-principles calculations give the Bloch wave velocities $\mathbf{v}_{ijs}$. The boundary conditions give the coefficients $F_{ijs}^{\pm}$.

The conservation of the number of electrons across each interface creates the boundary conditions. The transmission (T_i^{++},T_i^{--}) and reflection (T_i^{+-},T_i^{-+}) coefficients, determined from the first-principles calculations, express the relationship between the distribution functions in layer i and $i+1$ with an interface at z_i. Since the metallic layers are pseudomorphic, $\mathbf{k}_\parallel$ is conserved across the interface and the boundary conditions become

$$h_{i+1,s}^{+,j}(z_i^+,\mathbf{k}_\parallel) = S_{is}\left[\sum_{j'} T_{is}^{++}(j,j')h_{i,s}^{+,j'}(z_i^-,\mathbf{k}_\parallel) + T_{is}^{+-}(j,j')h_{i+1,s}^{-,j'}(z_i^+,\mathbf{k}_\parallel)\right],$$

$$h_{i,s}^{-,j}(z_i^-,\mathbf{k}_\parallel) = S_{is}\left[\sum_{j'} T_{is}^{-+}(j,j')h_{i,s}^{+,j'}(z_i^-,\mathbf{k}_\parallel) + T_{is}^{--}(j,j')h_{i+1,s}^{-,j'}(z_i^+,\mathbf{k}_\parallel)\right]. \qquad (2)$$

As an example of what these terms represent, $T_{is}^{-+}(j,j')$ corresponds to the probability that an electron with spin s, initially moving in the positive z direction in a state j', is reflected off the interface at z_i into a state moving in the negative z direction in a state j. A spin-dependent specularity parameter S_{is} (or P_i) scales the boundary conditions to reflect the degree of diffuse scattering on the interfaces. When the interface corresponds to an outer surface, the specularity parameter is symbolized by P_i. $P=1$ and $S=1$ correspond to completely specular scattering at the surfaces or interfaces, while $P=0$ and $S=0$ correspond to completely diffuse scattering. For a more detailed description of the model, see Ref. 20.

The conductivity is calculated from Eq. (1) with the boundary conditions (2). The measured conductivities were fitted using the following adjustable parameters: the bulk relaxation times $\tau_\uparrow$ and $\tau_\downarrow$ in each layer, the specular reflection coefficients P_0 and P_1 at the outer surfaces of the film, and the spin-dependent specularity parameters $S_\uparrow$ and $S_\downarrow$ for each interface.

B. Single Fe films

Fe films in the thickness range of 28–611 Å were grown on RT *GaAs*(001)-4×6 substrates as discussed in Sec. II. For the *in situ* transport measurements of the Fe films, however, the As that segregated to the top Fe surface was not sputtered away. The growth was interrupted at various intervals so that the sample could be retracted into a separate chamber in order to perform *in situ* four-probe resistance measurements. Based on thermocouple readings, the temperature of the sample during the resistance measurements was 300 K. The number of interruptions per sample was no more than three for the data presented in Fig. 4(a) in order to minimize the contamination of the surface by residual gases present in the chamber. Both carbon and oxygen eventually accumulated on the surface. Samples that experienced prolonged exposure to the residual gases, due to hour-long interruptions in the growth, did not show an increase in their resistivity compared to samples that were grown without interruption. This suggested that the contaminants remained on the surface during the growth and a negligible fraction were incorporated into the film. There were two important points to note about Fig. 4. (i) The conductivity approached the bulk conductivity of Fe at 300 K, $\sigma_{\mathrm{Fe}}=10.2(\mu\Omega\ \mathrm{m})^{-1}$, which indicated a high film quality with a low density of bulk defects. (ii) The conductivity approached this saturation value on a rather long length scale of 160 Å.

The conductivity was fitted using the Boltzmann model to extract the following four parameters: the relaxation times $\tau_\uparrow$ and $\tau_\downarrow$ and reflection coefficients P_i at both the Fe/GaAs and the Fe/vacuum interfaces. The fit was performed by first fixing the reflection coefficients to zero. In order to obtain the correct saturation value, the relaxation times were constrained to give the bulk conductivity of Fe. The remaining degree of freedom, the spin-asymmetry parameter $\alpha=\tau_\uparrow/\tau_\downarrow$, fitted the slow approach to saturation observed in the data. For the purposes of discussion the relaxation times were converted into mean free paths λ by multiplying by the average Fermi velocities. For $\alpha=1$, the correct bulk conductivity σ_{Fe}

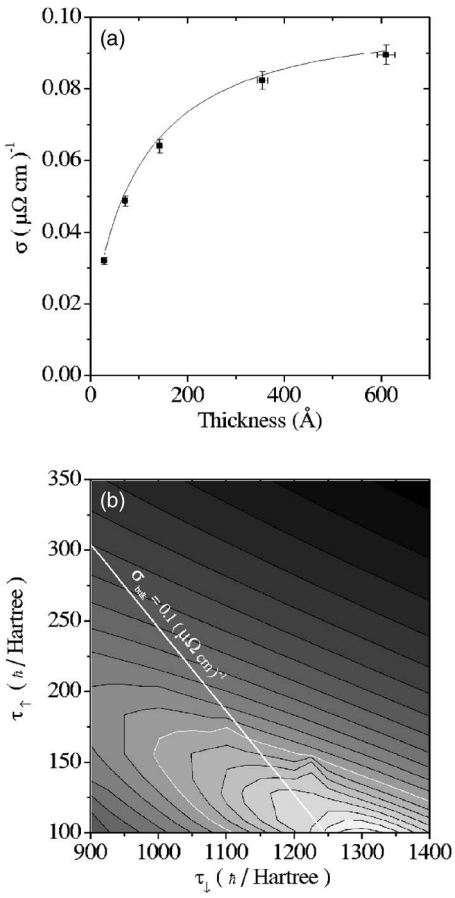

FIG. 4. (a) The *in situ* thickness dependence of the conductivity of Fe deposited on GaAs(001). The solid line was a fit to the data using first-principles calculations. The scattering parameters at both interfaces were fixed to be purely diffuse. The relaxation times determined from the fit were $\tau_{\downarrow}=(3.0\pm0.2)\times10^{-14}$ s and $\tau_{\uparrow}=(2.5\pm1.2)\times10^{-15}$ s. (b) The contour plot shows $\log_{10}(\chi^2)$ of the fit as a function of the scattering rates for minority and majority electrons. The scattering rates are given in units of $\hbar$/hartree $=2.42\times10^{-17}$ s. The straight white line indicates the combinations of relaxation times that yield the bulk conductivity of Fe. The white contour indicates the 90% confidence level of the fit.

is given by $\lambda_{\uparrow}=56$ Å and $\lambda_{\downarrow}=48$ Å. These mean free paths are far too short to fit the data. The slow approach to saturation was indicative of a large difference in relaxation times. To understand the reason for this it was useful to consider the dependence of the bulk conductivity on the mean free paths: $\sigma_{\mathrm{Fe}}=C^0_{\downarrow}\lambda_{\downarrow}+C^0_{\uparrow}\lambda_{\uparrow}$. From the first-principles code one found $C^0_{\downarrow}=6.30\times10^{14}$ $(\Omega\ \mathrm{m}^2)^{-1}$ and $C^0_{\uparrow}=1.26\times10^{15}$ $(\Omega\ \mathrm{m}^2)^{-1}$. If the spin asymmetry was adjusted so that current was only carried by majority electrons ($\lambda_{\downarrow}=0$), $\lambda_{\uparrow}=81$ Å gave the correct σ_{Fe}. On the other hand, if the spin asymmetry was adjusted so that the current was only carried by the minority electrons, $\lambda_{\uparrow}=0$, then $\lambda_{\downarrow}=162$ Å. Therefore one requires a large spin-down polarization of the carriers in order to explain the slow approach to saturation of the conductivity.

The conductivity was calculated for each of the five measured Fe thicknesses for all possible combinations of relaxation times $(\tau_{\uparrow},\tau_{\downarrow})$ between 2.4×10^{-15} and 3.4×10^{-14} s. The χ^2 of the fit was shown in Fig. 4(b) assuming complete diffuse scattering. The straight white line indicates the combinations of relaxation times that give the bulk conductivity, and therefore only values below this line are reasonable. From the χ^2, the best fit was found for $\tau_{\downarrow}=(3.0\pm0.2)\times10^{-14}$ s and $\tau_{\uparrow}=(2.5\pm1.2)\times10^{-15}$ s corresponding to a spin asymmetry parameter $\alpha=\tau_{\uparrow}/\tau_{\downarrow}=0.08\pm0.04$, and mean free paths $\lambda_{\downarrow}=(139\pm10)$ Å and $\lambda_{\uparrow}=(11\pm6)$ Å. It should be noted that the errors in the relaxation times were overestimates based on extrema of the 90% confidence interval. A more accurate representation of the error is given by the range of parameters that are both confined within the 90% confidence interval and that are below the line given by the bulk conductivity shown in Fig. 4(b). The calculation produced a good fit that as was shown in Fig. 4, with the exception of the conductivity at low thicknesses. The reason that the calculated conductivity at low film thickness is five standard deviations higher than the measured value may be due in part to quantum confinement effects.

The effect of quantum confinement on the transport was estimated by modifying the semiclassical calculation. The confinement was modeled by removing electrons from the integration whose half wavelengths were larger than the sample thickness d. Specifically, wave vectors with a component normal to the surface, $k_{\perp}$, satisfying the relation $k_{\perp}d<\pi$, were not included in the calculation. The modification to the calculation brought the calculated conductivity within three standard deviations of the measured conductivity of the 20-ML-thick Fe film, but it did not noticeably change the conductivity of larger thicknesses.

A second possible cause for the discrepancy between the data and the calculations could be due to the simplified treatment of the scattering. The calculation presented here used the relaxation time approximation, which assumes isotropic scattering. The scattered electrons in this case do not contribute to the current. Electrons that are scattered in the forward direction do, however, contribute to the conduction current. Butler *et al.*[20] and Penn *et al.*[22] showed that anisotropic scattering leads to a larger decrease in the conductivity at diffuse boundaries than predicted by the relaxation time approximation since there are fewer electrons available to scatter into the forward direction. According to Penn *et al.*, *p*-wave scattering in free-electron metals leads to a decrease in the conductivity by a factor of the order of 10% as compared to isotropic scattering.

By introducing a nonzero reflection coefficient the calculated conductivity approached saturation over a shorter length scale and the asymmetry had to be increased further to compensate with no improvement in the χ^2. Given the very large difference in relaxation times that was found by fitting the data with zero specularity at the outer interfaces, it was concluded that a nonzero P was unlikely.

The large spin asymmetry in relaxation times for Fe determined from the fit is surprising given what has been believed (by large asymmetry we mean α is much smaller than 1). It is interesting to compare what is expected based on Mott's interpretation of scattering. In his model the relaxation times are inversely proportional to the d density of states at the Fermi energy. From the density of states calculated from the same first-principles code used to calculate the conductivity, shown in Table I, the spin-asymmetry param-

TABLE I. The density of states at the Fermi level for majority and minority electrons in Fe calculated from the first-principles density functional code. The numbers are quoted in states/eV.

	s	p	d	f
↑	1.586×10^{-2}	3.26×10^{-2}	7.14×10^{-1}	3.816×10^{-3}
↓	3.256×10^{-2}	4.301×10^{-2}	2.72×10^{-1}	5.853×10^{-3}

eter was expected to be roughly $\alpha=0.38$. The large asymmetry (small α) based on this simple model was larger than was typically assumed.[23] However, the model could not fully account for the small value of α obtained from the fits.

We considered the effect Ga or As impurities would have on the conductivity. If these impurities were to diffuse into some region close to the Fe/GaAs interface then they would drop the local conductivity of this region. This would mean that the conductivity would approach saturation more slowly as a function of thickness and make the Fe appear to have a longer mean free path than it actually had. We tested this idea by using a free-electron model to calculate the conductivity of $Fe/Fe_{1-x}As_x$, where x is the concentration of As impurities in Fe. The $Fe_{1-x}As_x$ layer was assumed to be 30 Å thick and the $Fe_{1-x}As_x$/Fe interface was assumed to be perfectly transparent. The resistivity of the dirty layer was taken to be $9.8+8x$ ($\mu\Omega$ m).[24] For $x=0.1\%$, the upper limit of the As contamination given by XPS measurements, there is no significant change to the conductivity except for a drop in the conductivity for film thicknesses close in value to 30 Å. Therefore small As or Ga concentrations of the order of 0.1% may account for the fact that the measured conductivity at 30 Å is lower than first-principles calculations predict. This level of impurities, however, cannot account for the slow approach to saturation and hence the large difference in scattering rates. The calculations do show that if the impurity levels in the first 30 Å of our samples were as high as 1% (much higher than measured by XPS) they would have made the approach to saturation significantly slower than pure Fe and would have meant that the spin asymmetry in the Fe layer was actually $\alpha=0.2$. Even this value of α would be a factor of 2 larger than expected.

The high value of spin asymmetry reported in this article was also considerably greater than the asymmetry given by the experimental mean free paths for Fe in sputtered GMR structures, $\lambda_\uparrow=15$ Å and $\lambda_\downarrow=21$ Å, measured by Gurney *et al.*[23] These values corresponded to an asymmetry $\alpha=0.7$. It is, however, important to realize that the measurements made by Gurney *et al.*[23] were made on sputtered samples, which had a far greater number of defects that would have acted as sources of scattering. Interestingly the majority mean free path measured in sputtered samples, $\lambda_\uparrow=15\pm2$ Å, was within error of the value obtained for Fe/GaAs(001), $\lambda_\uparrow=11\pm6$ Å. The relatively low spin asymmetry reported in Ref. 23 can be explained by the presence of lattice defects in their polycrystalline samples. Basically a large mean free path for the minority electrons would be more affected by the lattice defects present in these samples than the majority electrons with a short mean free path.

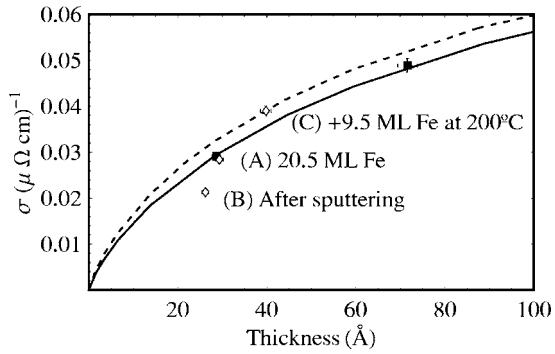

FIG. 5. The conductivity of Fe as a function of film thickness. The filled squares and the solid line are the data and the free-electron model fit with $P=0$, with the data from Fig. 4. The open diamonds labeled (A), (B), and (C) are the conductivities at various stages of the film preparation. The dashed line is a fit to point C with a reflectivity $P_{vac/Fe}=0.23$.

C. Transport in Au/Fe

The Au/Fe interface and the transport properties of Au are investigated by *in situ* measurement of the thickness dependence of the conductivity of a Au overlayer on a 28 ML Fe film. The Fe film was prepared by growing a 20.5-ML-thick layer at RT, sputtering away the As, and then growing a 9.5 ML Fe film at roughly 200 °C. The sheet resistance of the Fe film was measured for each step of the preparation and is shown in Fig. 5. The conductivity of the 20.5 ML Fe film grown at RT was within error of the value from a previous measurement. After sputtering, the conductivity drops well below the value expected from Fig. 4, which was attributed to damage created in the Fe lattice. The large increase in conductivity due to annealing and growth at elevated temperatures indicated that the defects due to the sputtering were repaired. The increase in the conductivity was explained by an increase in the specularity of the vacuum/Fe interface. The increase was quantified using a free-electron model. The model gave $\lambda=167$ Å for the Fe film prior to sputtering, assuming $P=0$ at both interfaces. The resulting fit is shown by the solid line in Fig. 5. After annealing and growth at elevated temperatures (point C in Fig. 5), the specularity of the outer Fe surface increased to $P_{vac/Fe}=0.23\pm0.10$.

The addition of a Au layer on the As-free Fe surface required four additional fitting parameters: the Au relaxation time, the spin-dependent specularity $S_\uparrow$ and $S_\downarrow$ for the Au/Fe interface, and the specularity parameters for the outer Au interface $P_{vac/Au}$. The thickness dependence of the conductivity for the Au/28 ML Fe bilayer is shown in Fig. 6. The fit was made by first noting that the conductivity approached the bulk value for Au, $\sigma_{Au}=0.44$ $(\mu\Omega\ \mathrm{cm})^{-1}$. The Au films on Fe/GaAs were assumed to have a relaxation time corresponding to pure Au. This is a reasonable assumption since the Fe relaxation times determined from Fig. 4 corresponded to the conductivity of pure Fe. A relaxation time $\tau=2.8\times10^{-14}$ s ($\lambda=380$ Å) was found by fitting the bulk conductivity with the first-principles calculations. This was in good agreement with the values predicted from the free-electron model. The relaxation times and the specularity $P_{Fe/GaAs}=0$ obtained from Fig. 4 were used to fit the data in Fig. 6. Only

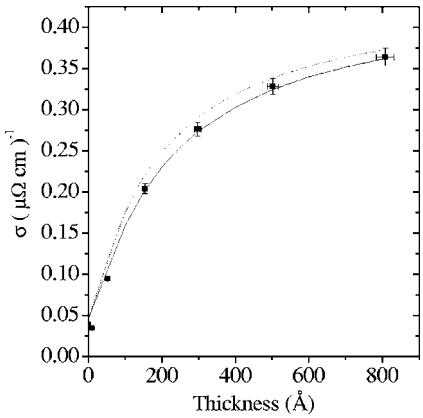

FIG. 6. *In situ* measurement of the conductivity as a function of Au thickness deposited on 28 ML Fe/GaAs(001). The two curves are calculated using first-principles density functional calculations. The solid line (P=0, $S_\uparrow$=0.55, $S_\downarrow$=0.77) is the best fit given the set of parameters described by line A in Fig. 7 below. The dashed line (P=0.41, $S_\uparrow$=0.03, $S_\downarrow$=0.65) has the highest χ^2 among the parameters on line A, which demonstrates the sensitivity of the fit to the fitting parameters.

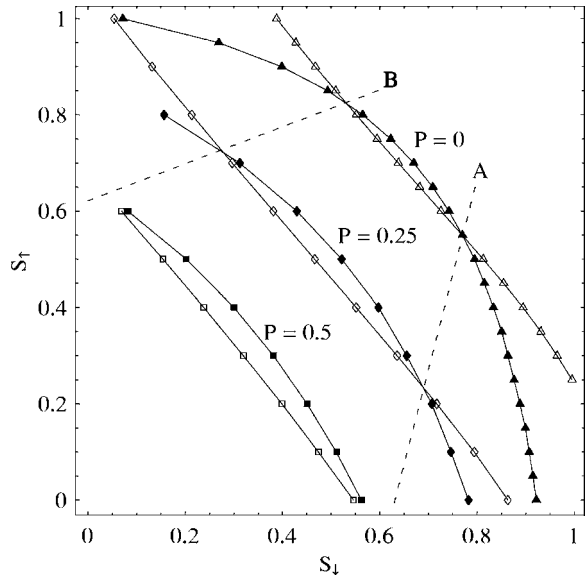

FIG. 7. Fitting of the conductivity of 20 ML Au/10 ML Fe/7 ML Au/28 ML Fe/GaAs(001) using first-principles calculations. The filled points correspond to the parameters which give the correct sheet resistance for a parallel configuration of magnetic moments (resistance at saturation in Fig. 2) and the open points give the correct sheet resistance for an antiparallel (zero applied field) configuration. The triangles, diamonds, and squares are calculated for $P_{\mathrm{vac/Au}}$=0, 0.25, and 0.5, respectively. The dashed lines labeled A and B are interpolations of the points of intersection which give the correct GMR.

three fitting parameters remained: $S_\uparrow, S_\downarrow$, and $P_{\mathrm{vac/Au}}$. Unfortunately a unique fit to the data was not achieved with the data in Fig. 6 alone.

The magnetoresistance data from Au/Fe/Au/Fe/GaAs(001) was used to help determine the specularity parameters. A necessary simplifying assumption that all Fe/Au interfaces had the same degree of specularity ($S_\uparrow$ and $S_\downarrow$) reduced the number of fitting parameters. The reflectivity at the outer Au interface $P_{\mathrm{vac/Au}}$ was first set to zero, and then all possible combinations of $S_\uparrow$ and $S_\downarrow$ that gave the correct conductivity for a parallel and antiparallel configuration in the Au/Fe/Au/Fe/GaAs sample were determined, as shown by the curves joining the two sets of triangles in Fig. 7. The points where these curves intersected gave the correct magnetoresistance. The calculation was repeated for $P_{\mathrm{vac/Au}}$ =0.25 and 0.50. The points of intersection for the various $P_{\mathrm{vac/Au}}$ lay roughly on straight lines, shown by the two dashed lines in Fig. 7. The specularity parameters decreased approximately linearly with increasing $P_{\mathrm{vac/Au}}$. The GMR data alone indicated that the reflection from the outer Au interface was mostly diffuse, $P_{\mathrm{vac/Au}}<0.5$, and one spin channel had a specularity in the range $0.6 \lesssim S \lesssim 0.8$.

Fits to Au conductivity data in Fig. 6 were subsequently constrained by the requirement that the parameters $P, S_\uparrow$ and $S_\downarrow$ produce the correct magnetoresistance for Au/Fe/Au/Fe (lines A and B in Fig. 7). P=0 gave the best fit to the Au conductivity. The solid line in Fig. 6 represents the fit to the data using either (P=0.0, $S_\uparrow$=0.55, and $S_\downarrow$=0.77) or (P =0.0, $S_\uparrow$=0.83, and $S_\downarrow$=0.53). When P was increased, the χ^2 also increased. The dashed line in Fig. 6 represents (P =0.41, $S_\uparrow$=0.03, and $S_\downarrow$=0.65), the fit having the highest χ^2 (satisfying the constraint of line A in Fig. 7). The results of the fits are displayed in Table II. A lower τ_{Au} would have resulted in larger specularity parameters.

The diffuse scattering modeled by $S_\uparrow$ and $S_\downarrow$ describe the influence of interface imperfections. Unfortunately, no calculations or measurements were available for the spin asymmetry of Au impurities in Fe for comparison to the fits. It was, however, interesting to compare the spin asymmetry of dilute Cu and Ag impurities in Fe since these elements were isoelectronic with Au and therefore were expected to scatter in a similar fashion. Mertig recently calculated a spin asymmetry $\rho^\downarrow/\rho^\uparrow$=8.20 for Cu and 12.22 for Ag.[25] This would suggest that Au defects at the Fe/Au interface would also diffusely scatter minority electrons more strongly. Based on this argument, one tends to favor the parameters from line A.

The fit of the Au thickness with first-principles calculation described the data well for large thicknesses, but failed to describe the conductivity for small thicknesses, in particular the 5 ML Au film. One had expected a drop in the conduc-

TABLE II. The GMR fitting parameters determined from Fig. 7 that gave the best fit to the thickness dependence of the Au conductivity shown in Fig. 6. The confidence interval column (CI) shown for each set of solutions A and B was the range of the specularity parameters within the 90% confidence interval of the fit. The 90% confidence interval is a region in the parameter space of χ^2 where 90% of experiments will be fitted by a set of parameters falling within that region.

	Best fit (A)	CI (A)	Best fit (B)	CI (B)
P	0.0	0.0–0.16	0.0	0.0–0.20
$S_\uparrow$	0.55	0.55–0.34	0.83	0.83–0.74
$S_\downarrow$	0.77	0.77–0.72	0.53	0.53–0.32

tivity at the initial stages of the Au growth based on some roughness associated with the formation of the vacuum/Au interface. Even with all of the specularity parameters set to zero, however, the calculations gave a conductivity of 0.043 $(\mu\Omega\,\mathrm{cm})^{-1}$ for 5 ML Au/28 ML Fe as compared to the measured value 0.037 ± 0.001 $(\mu\Omega\,\mathrm{cm})^{-1}$. This 20% difference could have been due to quantum mechanical confinement effects since a 10 Å Au film becomes comparable in size to the Fermi wavelength of the electrons. This observation is in agreement with those of Tešanovic *et al.* who demonstrated that the conductivity dropped more quickly at low thickness than the predictions based on the Boltzmann equation,[26] and that a full quantum mechanical treatment brought a better agreement in this regime. Another possible contribution to this discrepancy is anisotropic bulk scattering, as discussed in the previous section.

The highly diffuse scattering at the outer interfaces was responsible in part for the low GMR ratio. Given this diffuse scattering, we estimated what the GMR ratio would be if the Fe/Au interfaces were perfectly sharp. First-principles calculations of the GMR for diffuse scattering at the outer interfaces, and pure specular scattering at the inner interfaces ($P=0$, $S=1$), resulted in a GMR of 10%. The plots of the local conductance showed that the mechanism of the magnetoresistance in this case was the multiple reflections inside the Au spacer layer. The magnetoresistance was almost entirely confined to the spacer layer. The minority-spin channel was more reflecting than the majority. In a parallel configuration there were more reflections for minority electrons, and majority electrons leaked more into the ferromagnetic layers. In the antiparallel configuration both electrons were able to equally transmit through one of the interfaces. A relatively small decrease in specularity resulted in a large drop in magnetoresistance due to the decrease in the number of multiple reflections inside the spacer layer. This is analogous to a decrease of the quality factor of a resonator due to lossy walls.

D. Discussion of the scattering at the Au/Fe interfaces

There is an interesting symmetry in the two sets of fitting parameters given by Fig. 7. The GMR data and Au thickness data cannot distinguish which spin channel was more heavily scattered. This at first seemed to be a contradictory result. It was not immediately obvious how an asymmetry in the diffuse scattering could be insensitive to the large bulk spin asymmetry. One of the difficulties in using first-principles code is that the intrinsic transmission and reflection coefficients are hidden in the calculation; however, one has to consider these numbers in order to understand the unexpected insensitivity to the asymmetry in diffuse scattering. To gain some insight into the intrinsic scattering created at the Fe/Au interface, the first-principles calculations were compared to a free-electron model with wave-vector-independent transmission and reflection coefficients. Although the Fe could not be well described by a spherical Fermi surface, the Au spacer layer should be fairly well described by the free-electron theory. The free-electron model required small transmittivities $T_{\uparrow}=0.1$ and $T_{\downarrow}=0.05$ to obtain the same local conductivity in the spacer layer as calculated by first-principles calculations. The low transmission coefficients are in qualitative agreement with the calculations of Stiles.[27] For current in-plane (CIP) GMR, the electrons propagating in a direction close to the interface normal (or near the interface zone center) contribute little to the magnetoresistance. Stiles showed that for Fe/Au interfaces the electrons at the edges of the interface zone, those important for CIP GMR, have a low transmission coefficient.

The reason that the data could not distinguish between the two sets of diffuse scattering parameters was a result of the small transmission coefficients. The large mismatch between Fe and Au produces a situation where the Fe films are mostly uncoupled from a transport point of view.

Given that the asymmetry in the relaxation times were as large as those estimated for Co, one may ask why Fe/Cu or Fe/Au multilayers have a much lower GMR ratio than Co/Cu multilayers. GMR ratios in Co/Cu are as large as 65%,[28] whereas Fe/Cu and Fe/Au multilayers are only a few percent. The important difference between these systems is that the Co majority-electron band is well matched to the Cu *s-p* band,[20,29,30] whereas the minority band is not. It was suggested by Dieny[31] that the source of the small GMR in Fe/Cu is due to the poor mismatch between the Fe and Cu band structures for both majority and minority electrons. In the case of Fe/Au, first-principles calculations of the local conductance indicated that both spin channels are poorly matched for the k vectors responsible for CIP GMR,[27] and therefore there is not a large change in resistance between a parallel and an antiparallel alignment of the magnetic moments. Co/Cu is a unique case. Although the Fermi surfaces of Au and Cu are very similar, where Au is only about 10% smaller than Cu, Co/Au systems have a very small GMR of the order of 1%.[32] This points to influences other than the electronic structure which gave rise to the magnetoresistance. In a comparison between experimentally measured exchange coupling strengths in heterogeneous spacers and layer KKR first-principles calculations, it was found that matching of the atomic size was an important consideration.[33] By placing a Ag layer inside a Cu spacer the exchange coupling strength was reduced. Calculations could only reproduce the decrease in coupling when both the electronic structure and the atomic size were accounted for. The change in the electronic density associated with the larger Ag atoms led to increased reflectivity from the Cu/Ag interface.[33] The poor GMR ratios in Co/Au are likely due to the same effect. And likewise in the case of Au, the mismatch in atom sizes between Fe and Au is expected to increase the reflectivity from the Fe/Au interfaces.

V. SCATTERING AT THE OUTER INTERFACES

A surprising result of the fit was the zero specular reflectivity. Given that the Fermi wavelength of the electrons was of the order of 1 Å, and the terrace of the GaAs substrate and the outer Au surface were hundreds of angstroms long, one would have expected considerable specular scattering from the outer interfaces.

The scattering inside the crystal is due to the random variations in potentials. In the bulk, these variations are typi-

cally caused by point defects and lattice vibrations. At a perfect surface, the potential is uniform and all electrons are reflected in phase with one another. Surface roughness creates random variations in the surface height function. The variations in height translate into variations in the electron path lengths of those electrons reflected from the surface. Ziman[34] and Soffer[35] have shown that this is analogous to the surface diffraction problem.

In the following, the diffraction of conduction electrons is calculated using a model where each surface atom has the same scattering potential. This model determines the contribution to scattering resulting from the interference of the electron wave functions reflected from different step heights. As discussed in Ref. 35, in order to formulate surface diffraction for electron transport using an Ewald construction, the electron wave packet was assumed to be large enough so as to have a nearly monochromatic wavelength. From the STM pictures in Fig. 1, the reciprocal space was calculated by taking the Fourier transform of the surface, $A(\mathbf{K})$. The intersection of the Fermi surface (which took the role of the Ewald sphere) with the calculated diffraction intensity distribution $S(\mathbf{K})=|A(\mathbf{K})|^2$ yielded the angular distribution of reflected electrons.

In the case of Au, a spherical Fermi surface was used with a radius equal to the free electron wave vector $k_F=1.21\times10^8$ cm^{-1}. The reflected intensity distribution calculated from the STM image of 20 ML Au/28 ML Fe/GaAs(001) was presented for three angles of incidence. The diffraction intensity in the plane of incidence for three different angles of incidence was plotted in Fig. 8. A large fraction of the intensity was found to be specular, and most of the diffuse scattering was just off specular. The reflection coefficient for a given angle of incidence could be estimated by taking the ratio of the specular intensity to the integration of the total reflection distribution. Since it was hard to distinguish the specular peak from the off-specular diffuse shoulder, a conservative estimate was made by taking the intensity above 2500 units to be specular and the remainder was considered diffuse. For angles of incidence $\theta=23°$, 45°, and 72° the reflection coefficients were 0.4, 0.55, and 0.8, respectively. One should keep in mind that this was a representation of the fraction of the electrons which were exactly specular. Most of the intensity was not scattered in random directions, but was highly focused near the specular direction. These electrons did not lose complete memory of their original momentum and hence contributed to the current. In other words, it was expected from the calculation that the outer Au interface would have had a very large degree of specular scattering.

The small reflection coefficient that was observed for the Au surface may be a result of the 5×1 reconstruction visible in Fig. 1(c). The calculation of the scattering directly from the Fourier transform of the surface gives the contribution of the diffraction only as a result of the height variations of the buckled surface, but it does not account for variations in the scattering potential as a result of this buckling. The discrepancy between the fitted reflection coefficients and kinematical calculations of the scattering indicate that a site-specific scattering potential may be required to understand the diffuse scattering from the surfaces of thin films.

From the STM pictures of the GaAs surface, one might have also expected large specular scattering from the Fe/GaAs interface. From the observation of As segregation, however, it was clear that the deposition of Fe did disrupt the GaAs surface. Perhaps the length scale of this perturbation was on a length scale short enough to have caused purely diffuse scattering at the Fe/GaAs interface.

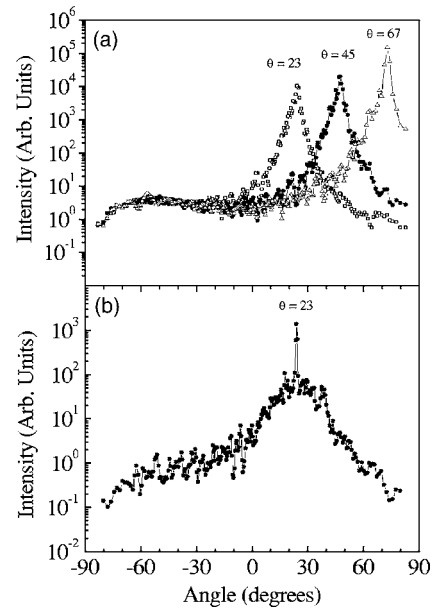

FIG. 8. (a) The calculated reflectivity from the STM image in Fig. 1(c) of 20 ML Au/28 ML Fe/GaAs(001). The reflectivity as a function of the polar angle is plotted with respect to the surface normal for three angles of incidence ($\theta=0.23°$, 0.45°, and 0.72°). The large peak corresponds to the specular component of the reflection. (b) The calculated reflectivity from the STM image in Fig. 1(a) of 20 ML Fe/GaAs(001). The reflectivity as a function of the polar angle is plotted with respect to the surface normal. The large peak corresponds to the specular component of the reflection.

To investigate the scattering from the As-covered Fe surface, the same calculation performed for the Au surface was repeated for a 20 ML Fe film on GaAs(001). In the case of Fe, however, the Fermi surface was much more complicated. There are four different Fermi sheets which were far from being spherical.[37] As a crude approximation to simplify calculations, the Fermi surface of Fe was taken to be a single spherical Fermi surface of radius $k_F=1\times10^8$ cm^{-1}. The reflected intensity distribution was calculated for an angle of incidence $\theta=23°$ and is shown in Fig. 8. The figure showed a sharp peak with a diffuse intensity distribution centered around the specular direction. Integration of the distribution gave a reflection coefficient of $P=0.3$.

The difference in calculated and fitted reflection coefficients perhaps points to a failure of the scattering model that was used. The kinematical model used here treated each scatterer on an equal footing. Localized surface states have not been taken into account by the kinematical model; these states could effect the scattering from defect sites. Furthermore, atoms at step edges tend to scatter electrons more strongly. This is reminiscent of the question of the origin of RHEED intensity oscillations from a growing surface. One model proposes that the cause for RHEED oscillations is variations in the interference between electrons reflected

from different step heights as islands nucleate and coalesce. A second model attributes it to variations in the diffuse scattered intensity due to oscillations in the step density of the growing surface. Similarly, this work raises the question of what fraction of the conduction electron scattering is coherent and what portion is due to variations in the defect potentials.

VI. CONCLUSION

The *in situ* thickness dependence of the conductivity of epitaxial Fe films grown on GaAs(001) and Au grown on Fe/GaAs(001) demonstrated that these films have the conductivity of bulk samples, reduced only by the presence of interfaces. Surprisingly, a small spin-asymmetry parameter $\alpha=0.08\pm0.04$ was required to fit the thickness dependence of the conductivity of the Fe films. Fits to the conductivity of Fe, Au/Fe, and Au/Fe/Au/Fe films using first-principles calculations show a low degree of specular scattering at the outer interfaces. This is in contrast to the predictions of nearly perfect specular scattering based on kinematical calculations using the STM data.

The low GMR observed in Fe/Au/Fe was in part due to the diffuse scattering at the outer interfaces. A comparison between experiment and first-principles calculations has given insight into the magnetoresistance of Fe/Au that would not have been possible otherwise. The calculations showed that the low GMR observed in Au/Fe structures is due to the high reflectivity of both spin channels at the Fe/Au interfaces. The nature of this reflectivity is a result of a mismatch in electronic structure between Fe and Au. GMR in Fe/Au was found to arise from multiple reflections within the spacer layer, known as the waveguide effect, or spin channeling. The spin asymmetry in reflectivities is predicted to be large enough to produce a moderate 10% GMR in our quadrilayer structures if the Fe/Au interfaces had been ideal. The small degree of diffuse scattering at the inner interfaces, however, substantially reduced the number of multiple reflections within the Au spacer and led to a further decrease of the GMR.

ACKNOWLEDGMENTS

The authors would like to thank M. D. Stiles for helpful discussions and C. Bolognesi and D. DiSanto for the photolithographic patterning of our samples. T.L.M. gratefully acknowledges the Natural Sciences and Engineering Research Council for their financial support. This work was supported in part by Laboratory Directed Research and Development funds at Oak Ridge National Laboratory and by the Office of Basic Energy Sciences Division of Materials Sciences of the U.S. Department of Energy. Oak Ridge National Laboratory is operated by UT-Battelle, LLC, for the U.S. Department of Energy under Contract No. DE-AC05-00OR22725.

*Also affiliated with Metals and Ceramics Division, Oak Ridge National Laboratory, P.O. Box 2008, Oak Ridge, Tennessee 37831-6114.

[1] P. Baumgart, B. A. Gurney, D. R. Wilhoit, T. Nguyen, B. Dieny, and V. Speriosu, J. Appl. Phys. **69**, 4792 (1991).
[2] S. S. P. Parkin, Phys. Rev. Lett. **71**, 1641 (1993).
[3] M. Suzuki and Y. Taga, Phys. Rev. B **52**, 361 (1995).
[4] M. J. Hall, B. J. Hickey, M. A. Howson, M. J. Walker, D. Greig, and N. Wiser, J. Magn. Magn. Mater. **121**, 421 (1993).
[5] E. E. Fullerton, D. M. Kelly, J. Guimpel, I. K. Schuller, and Y. Bruynseraede, Phys. Rev. Lett. **68**, 859 (1992).
[6] R. Schad, P. Beliën, G. Verbanck, V. V. Moshchalkov, Y. Bruynseraede, H. E. Fischer, S. Lefebvre, and M. Bessiere, Phys. Rev. B **59**, 1242 (1999).
[7] P. M. Levy, S. Zhang, and A. Fert, Phys. Rev. Lett. **65**, 1643 (1990).
[8] T. L. Monchesky, B. Heinrich, R. Urban, K. Myrtle, M. Klaua, and J. Kirschner, Phys. Rev. B **60**, 10242 (1999).
[9] T. L. Monchesky, R. Urban, B. Heinrich, M. Klaua, and J. Kirschner, J. Appl. Phys. **87**, 5167 (2000).
[10] G. K. Binnig, H. Rohrer, C. Gerber, and E. Stoll, Surf. Sci. **144**, 321 (1984).
[11] A. M. Begley, S. K. Kim, J. Quinn, F. Jona, H. Over, and P. M. Marcus, Phys. Rev. B **48**, 1779 (1993).
[12] Y.-L. He and G.-C. Wang, Phys. Rev. Lett. **71**, 3834 (1993).
[13] F. J. Himpsel, Phys. Rev. B **44**, 5966 (1991).
[14] J. Unguris, R. J. Celotta, and D. T. Pierce, Phys. Rev. Lett. **79**, 2734 (1997).
[15] J. F. Cochran, J. Magn. Magn. Mater. **147**, 101 (1995).
[16] B. Heinrich and J. F. Cochran, Adv. Phys. **42**, 523 (1993).
[17] P. Grünberg, A. Fuss, Q. Leng, R. Schreiber, and J. A. Wolf, *Magnetism and Structure in Systems of Reduced Dimensions*, NATO Advanced Studies Institute, Series B: Physics (Plenum Press, New York, 1993), Vol. 309.
[18] K. Shintaku, Y. Daitoh, and T. Shinjo, Phys. Rev. B **47**, 14584 (1993).
[19] S. Honda, K. Koguma, M. Nawate, and I. Sakamoto, J. Appl. Phys. **82**, 4428 (1997).
[20] W. H. Butler, X.-G. Zhang, and J. M. MacLaren, J. Supercond. **13**, 221 (2000).
[21] J. M. MacLaren, X.-G. Zhang, W. H. Butler, and X. Wang, Phys. Rev. B **59**, 5470 (1999).
[22] D. R. Penn and M. D. Stiles, Phys. Rev. B **59**, 13338 (1999).
[23] B. A. Gurney, V. S. Speriosu, J.-P. Nozieres, H. Lefakis, D. R. Wilhoit, and O. U. Need, Phys. Rev. Lett. **71**, 4023 (1993).
[24] R. M. Bozorth, *Ferromagnetism* (D. Van Nostrand Company, Princeton, NJ, 1978).
[25] I. Mertig, Rep. Prog. Phys. **62**, 237 (1999).
[26] Z. Tešanović, M. V. Jarić, and S. Maekawa, Phys. Rev. Lett. **57**, 2760 (1986).
[27] M. D. Stiles, J. Appl. Phys. **79**, 5805 (1996).
[28] S. S. P. Parkin, Z. G. Li, and D. J. Smith, Appl. Phys. Lett. **58**, 2710 (1991).
[29] J. Mathon, M. Villeret, R. B. Muniz, J. d'Albuquerque e Castro, and D. M. Edwards, Phys. Rev. Lett. **74**, 3696 (1995).
[30] P. Bruno, Phys. Rev. B **52**, 411 (1995).

[31] B. Dieny, J. Magn. Magn. Mater. **136**, 335 (1994).
[32] J. Barnaś, A. Fuss, R. E. Camley, P. Grünberg, and W. Zinn, Phys. Rev. B **42**, 8110 (1990).
[33] M. M. Z. Kowalewski, Ph.D. thesis, Simon Fraser University, 1998.
[34] J. M. Ziman, *Electrons and Phonons: The Theory of Transport Phenomena in Solids* (Oxford University Press, Oxford, 1960).
[35] S. B. Soffer, J. Appl. Phys. **38**, 1710 (1967).
[36] The simulation was made using SRIM-2000.39 software, which can be downloaded from http://www.srim.org
[37] For Fermi surfaces of Fe and other elements, see the web page http://www.phy.tu-dresden.de/~fermisur